# *Skill assessment and sources of predictability for the leading modes of sub-seasonal Eastern Africa short rains variability*

Article

Accepted Version

de Andrade, F. M., Hirons, L. C. ORCID: https://orcid.org/0000-0002-1189-7576 and Woolnough, S. J. ORCID: https://orcid.org/0000-0003-0500-8514 (2024) Skill assessment and sources of predictability for the leading modes of sub-seasonal Eastern Africa short rains variability. Climate Dynamics. ISSN 1432-0894 doi: 10.1007/s00382-024-07244-9 Available at https://reading-clone.eprints-hosting.org/116132/

It is advisable to refer to the publisher's version if you intend to cite from the work. See Guidance on citing.

To link to this article DOI: http://dx.doi.org/10.1007/s00382-024-07244-9

Publisher: Springer

All outputs in CentAUR are protected by Intellectual Property Rights law, including copyright law. Copyright and IPR is retained by the creators or other copyright holders. Terms and conditions for use of this material are defined in the End User Agreement.

www.reading.ac.uk/centaur

**CentAUR**

Central Archive at the University of Reading

Reading's research outputs online

# Metadata of the article that will be visualized in OnlineFirst

| | | |
|---|---|---|
| ArticleTitle | Skill assessment and sources of predictability for the leading modes of sub-seasonal Eastern Africa short rains variability | |
| Article Sub-Title | | |
| Article CopyRight | The Author(s), under exclusive licence to Springer-Verlag GmbH Germany, part of Springer Nature (This will be the copyright line in the final PDF) | |
| Journal Name | Climate Dynamics | |


| | | |
|---|---|---|
| Corresponding Author | FamilyName | **Andrade** |
| | Particle | de |
| | Given Name | **Felipe M.** |
| | Suffix | |
| | Division | National Centre for Atmospheric Science and Department of Meteorology |
| | Organization | University of Reading |
| | Address | Reading, UK |
| | Division | |
| | Organization | National Institute for Space Research |
| | Address | Cachoeira Paulista, SP, Brazil |
| | Phone | |
| | Fax | |
| | Email | felipestratus@gmail.com |
| | URL | |
| | ORCID | http://orcid.org/0000-0001-6653-3916 |
| Author | FamilyName | **Hirons** |
| | Particle | |
| | Given Name | **Linda C.** |
| | Suffix | |
| | Division | National Centre for Atmospheric Science and Department of Meteorology |
| | Organization | University of Reading |
| | Address | Reading, UK |
| | Phone | |
| | Fax | |
| | Email | |
| | URL | |
| | ORCID | http://orcid.org/0000-0002-1189-7576 |
| Author | FamilyName | **Woolnough** |
| | Particle | |
| | Given Name | **Steven J.** |
| | Suffix | |
| | Division | National Centre for Atmospheric Science and Department of Meteorology |
| | Organization | University of Reading |
| | Address | Reading, UK |
| | Phone | |
| | Fax | |
| | Email | |
| | URL | |
| | ORCID | http://orcid.org/0000-0003-0500-8514 |



| | | |
|---|---|---|
| Schedule | Received | 8 Jan 2024 |
| | Revised | |

| | | |
|---|---|---|
| | Accepted | 12 Apr 2024 |

| | |
|---|---|
| Abstract | Understanding how models represent sub-seasonal rainfall variations and what influences model skill is essential for improving sub-seasonal forecasts and their applications. Here, empirical orthogonal function (EOF) analysis is employed to investigate weekly Eastern Africa short rains variability from October to December. The observed leading EOF modes are identified as (i) a monopole-like rainfall pattern with anomalies impacting southern Ethiopia, Kenya, and northern Tanzania; and (ii) a dipole-like rainfall pattern with contrasting anomalies between Tanzania and the northeastern sector of Eastern Africa. An examination of the links between the leading modes and specific climate drivers, namely, the Madden–Julian Oscillation (MJO), El Niño–Southern Oscillation, and Indian Ocean Dipole (IOD), shows that the MJO and IOD have the highest correlations with the two rainfall modes and indicates that the monopole (dipole)-like rainfall pattern is associated with MJO convective anomalies in the tropical Indian Ocean and western Pacific (Maritime Continent and Western Hemisphere). Assessments of model ability to capture and predict the leading modes show that the European Centre for Medium-Range Weather Forecasts (ECMWF) and the UK Met Office models outperform the National Centers for Environmental Prediction model at forecast horizons from one to four weeks ahead. Amongst the drivers examined, the MJO has the largest impact on the forecast skill of rainfall modes within the ECMWF model. If MJO-related variability is reliably represented, the ECMWF model is more skilful at predicting the main modes of weekly rainfall variability over the region. Our findings can support model developments and enhance anticipatory planning efforts in several sectors, such as agriculture, food security, and energy. |

| | |
|---|---|
| Keywords (separated by '-') | Eastern Africa Short Rains - Empirical Orthogonal Function Analysis - Madden–Julian Oscillation - El Niño-Southern Oscillation - Indian Ocean Dipole - Sub-seasonal Prediction Skill |
| Footnote Information | |

Climate Dynamics
https://doi.org/10.1007/s00382-024-07244-9

# Skill assessment and sources of predictability for the leading modes of sub-seasonal Eastern Africa short rains variability

**Felipe M. de Andrade**[1,2] · **Linda C. Hirons**[1] · **Steven J. Woolnough**[1]

Received: 8 January 2024 / Accepted: 12 April 2024
© The Author(s), under exclusive licence to Springer-Verlag GmbH Germany, part of Springer Nature 2024

UNCORRECTED PROOF

## Abstract

Understanding how models represent sub-seasonal rainfall variations and what influences model skill is essential for improving sub-seasonal forecasts and their applications. Here, empirical orthogonal function (EOF) analysis is employed to investigate weekly Eastern Africa short rains variability from October to December. The observed leading EOF modes are identified as (i) a monopole-like rainfall pattern with anomalies impacting southern Ethiopia, Kenya, and northern Tanzania; and (ii) a dipole-like rainfall pattern with contrasting anomalies between Tanzania and the northeastern sector of Eastern Africa. An examination of the links between the leading modes and specific climate drivers, namely, the Madden–Julian Oscillation (MJO), El Niño–Southern Oscillation, and Indian Ocean Dipole (IOD), shows that the MJO and IOD have the highest correlations with the two rainfall modes and indicates that the monopole (dipole)-like rainfall pattern is associated with MJO convective anomalies in the tropical Indian Ocean and western Pacific (Maritime Continent and Western Hemisphere). Assessments of model ability to capture and predict the leading modes show that the European Centre for Medium-Range Weather Forecasts (ECMWF) and the UK Met Office models outperform the National Centers for Environmental Prediction model at forecast horizons from one to four weeks ahead. Amongst the drivers examined, the MJO has the largest impact on the forecast skill of rainfall modes within the ECMWF model. If MJO-related variability is reliably represented, the ECMWF model is more skilful at predicting the main modes of weekly rainfall variability over the region. Our findings can support model developments and enhance anticipatory planning efforts in several sectors, such as agriculture, food security, and energy.

**Keywords** Eastern Africa Short Rains · Empirical Orthogonal Function Analysis · Madden–Julian Oscillation · El Niño-Southern Oscillation · Indian Ocean Dipole · Sub-seasonal Prediction Skill

## 1 Introduction

Rainfall variations in Eastern Africa, which includes the countries of Burundi, Djibouti, Eritrea, Ethiopia, Kenya, Rwanda, Somalia, Sudan, South Sudan, Tanzania, and Uganda (Fig. 1), with a total population of 457 million people (Palmer et al. 2023), may substantially impact several crucial activities in the region, in sectors such as agriculture, food security, and energy (Funk et al. 2008; Anande and Luhunga 2019; Chang'a et al. 2020; FSNAU 2022; Palmer et al. 2023). Thus, there has been an increasing interest in understanding what controls Eastern Africa rainfall variability (Ogallo et al. 1988; Ogallo 1989; Indeje et al. 2000; Black et al. 2003; Schreck and Semazzi 2004; Bowden and Semazzi 2007; Berhane and Zaitchik 2014; Gamoyo et al. 2015; Nicholson 2017; Wenhaji Ndomeni et al. 2018; Kolstad and MacLeod 2022; Maybee et al. 2022; among others).

Specifically, significant variations in Eastern Africa rainfall occur throughout the October–November-December (OND) short rains (Nicholson 2017; Palmer et al. 2023), showing, in particular, large interannual/seasonal variability (Camberlin and Wairoto 1997; Camberlin et al. 2009). Previous studies have investigated the sources of seasonal short rains variability, mainly indicating associations with El Niño-Southern Oscillation (ENSO; Nicholson and Kim 1997; Schreck and Semazzi 2004; Bowden and Semazzi 2007; Hoell et al. 2014; MacLeod et al. 2021; Kolstad and

✉ Felipe M. de Andrade
felipestratus@gmail.com

[1] National Centre for Atmospheric Science and Department of Meteorology, University of Reading, Reading, UK

[2] National Institute for Space Research, Cachoeira Paulista, SP, Brazil



Journal : Large 382 | Article No : 7244 | Pages : 17 | MS Code : 7244 | Dispatch : 19-4-2024

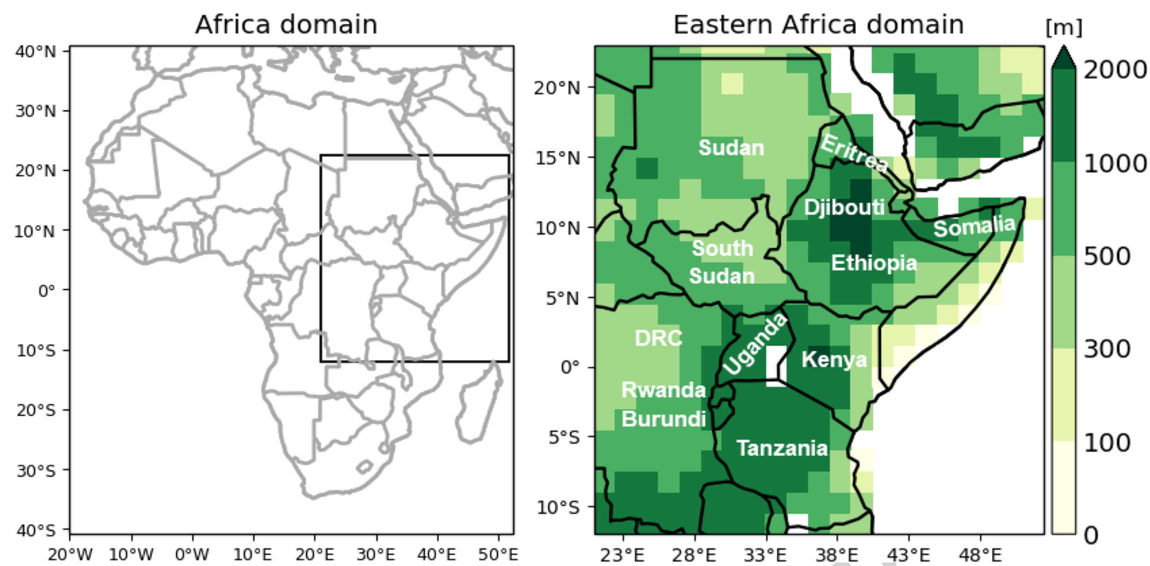


**Fig. 1** Africa domain in the left panel with a black box indicating the Eastern Africa domain (12ºS-23ºN, 21°-52.ºE) magnified in the right panel. Burundi, Djibouti, Eritrea, Ethiopia, Kenya, Rwanda, Somalia, Sudan, South Sudan, Tanzania, and Uganda are the 11 countries comprising the Eastern Africa domain. DRC stands for Democratic Republic of the Congo. Topography (shaded) in the right panel is shown in metres (m) and sourced from ERA5 reanalysis (Hersbach et al. 2020)

MacLeod 2022) and the Indian Ocean Dipole (IOD; Black et al. 2003; Behera et al. 2005; Nicholson 2015; Hirons and Turner 2018; Bahaga et al. 2019; Kolstad and MacLeod 2022). Strong co-variability exists between ENSO and the IOD (Nicholson 2015; Zhang et al. 2015), with the latter typically having more influence than the former on the short rains owing to its modulation of local zonal circulation (Goddard and Graham 1999; Bergonzini et al. 2004; Nicholson 2015; Zhao and Cook 2021). A weaker-than-normal zonal circulation over the Indian Ocean is related to positive sea surface temperature (SST) anomalies in the west and negative SST anomalies in the east, leading to enhanced rainfall in Eastern Africa (Black et al. 2003; Behera et al. 2005; Ummenhofer et al. 2009). The opposite SST pattern strengthens the zonal circulation over the Indian Ocean (Jiang et al. 2021; Zhao and Cook 2021), favouring reduced rainfall in Eastern Africa (Black et al. 2003; Behera et al. 2005). The most recent noticeable impact of an IOD event occurred in Eastern Africa's 2019 short rains and was associated with substantially above-average rains that forced hundreds of thousands of people to flee their homes and caused crop and livestock losses in the areas severely affected (Wainwright et al. 2021).

In addition to seasonal rainfall variability, sub-seasonal short rains anomalies (i.e., wet and dry spells within the rainy season that extend longer than the synoptic timescale) have also been identified (Camberlin and Wairoto 1997; Mutai and Ward 2000; Pohl and Camberlin 2006a; b; Zaitchik 2017). Such sub-seasonal rainfall variations are mainly related to the influence of the Madden–Julian Oscillation (MJO) over Eastern Africa, with significant phasing dependence (Pohl and Camberlin 2006a; b; Omeny et al. 2008; Berhane and Zaitchik 2014; Hogan et al. 2015). In general, rainfall increases (reduces) in most of Eastern Africa when the MJO-enhanced convective core is over the tropical Indian Ocean (Western Pacific) (Omeny et al. 2008; Hogan et al. 2015), as indicated by phases 2 and 3 (6 and 7) of the Real-Time Multivariate MJO index (RMM; Wheeler and Hendon 2004).

While seasonal predictions of short rains variability show great accuracy several months ahead of a season in association with ENSO and IOD modulation (Bahaga et al. 2015; MacLeod 2019; Walker et al. 2019), sub-seasonal prediction skill of short rains variability over a few weeks ahead remains relatively modest (Vigaud et al. 2018; 2019; de Andrade et al. 2021; Kolstad et al. 2021), with correlations rarely above 0.4 after two weeks lead time (de Andrade et al. 2021). As a result, linearly corrected forecasts have emerged and, to some extent, skill improvements have been linked to potential drivers of sub-seasonal to seasonal predictability such as the MJO, ENSO, and the IOD (Vigaud et al. 2018; de Andrade et al. 2021; Kolstad et al. 2021). Nevertheless, improving our understanding of sub-seasonal short rains variability, particularly the underlying drivers that modulate the local rainfall impacts, is essential to better predicting and anticipating sub-seasonal rainfall anomalies in Eastern Africa.

Here, an in-depth investigation of sub-seasonal variability and prediction skill of short rains is performed by examining its leading weekly rainfall modes rather than the




| | | | | |
|---|---|---|---|---|
| Journal : **Large 382** | Article No : **7244** | Pages : **17** | MS Code : **7244** | Dispatch : **19-4-2024** |

commonly assessed weekly rainfall anomalies within the season (Vigaud et al. 2019; de Andrade et al. 2021). This approach allows us to evaluate distinct weekly rainfall variability patterns accounting for the largest portion of the total variance in the sub-seasonal rainfall anomalies. While this approach has been applied in a small number of studies at pentad and seasonal timescales (Schreck and Semazzi 2004; Bowden and Semazzi 2007; Wenhaji Ndomeni et al. 2018; Kolstad and MacLeod 2022), evidence is lacking for further assessing the leading modes of Eastern Africa short rains variability at weekly timescales, along with their representation within dynamical models, sources of predictability, and prediction skill. Given that, the following questions are addressed:

What are the leading modes of weekly Eastern Africa short rains variability and their relationships with potential climate drivers?

What is the current ability of the models to capture and predict the leading rainfall modes at different weekly lead times?

What is the contribution of climate drivers to the sub-seasonal predictive skill of the leading rainfall modes?

Providing answers to the questions above would help advance the scientific understanding, support model developments, and contribute to assisting sectors in taking preparedness measures that reduce or avoid the effects of high-impact weather conditions on people's lives and livelihoods in Eastern Africa (Hirons et al. 2021; Gudoshava et al. 2022). The paper is organised as follows: Section 2 presents the datasets and methods used, Section 3 describes the results from this study, and Section 4 summarises key findings and provides conclusions.

## 2 Methodology

### 2.1 Observational analysis

Rainfall data sourced from the Tropical Applications of Meteorology using SATellite and ground-based observations (TAMSAT; Maidment et al. 2014; 2017) version 3.1 were used to investigate observed sub-seasonal Eastern Africa short rains variability. Land-only TAMSAT rainfall estimates are derived from rain gauge measurements used for calibration and thermal infrared satellite imagery (Maidment et al. 2017). Here, the spatial resolution of daily TAMSAT data was linearly interpolated (using bilinear interpolation) from the regular $0.0375° \times 0.0375°$ grid to $1.5° \times 1.5°$ to facilitate the comparison with modelled outputs, as shown later. Although TAMSAT produces rainfall estimates from 1983 to the present, we focused on the 1999–2016 period to match all datasets temporal resolution analysed here. Weekly data were obtained by averaging seven consecutive days without overlapping from October 1st to December 24th, totalling 13 weeks within the short rains season. This produces a sample size of 234 weeks between 1999 and 2016 (13 weeks over 18 years). Weekly rainfall anomalies were computed by subtracting the corresponding 1999–2016 long-term mean from the total field.

Given the known uncertainty in rainfall observations in the region (Sylla et al. 2013), three other observational datasets were assessed to examine how sensitive the results are to selecting the observational reference, following the method described to obtain weekly TAMSAT rainfall anomalies. The additional datasets are the land-only Climate Hazards Group Infrared Precipitation with Stations (CHIRPS; Funk et al. 2015), the Global Precipitation Climatology Project (GPCP; Huffman et al. 2001) version 1.3, and the Tropical Rainfall Measuring Mission (TRMM) Multi-Satellite Precipitation Analysis 3B42 (Huffman et al. 2007). These datasets were chosen because they are also frequently used satellite-derived products to study rainfall variability in Eastern Africa (Dinku et al. 2007; 2011; Kimani et al. 2017; Ageet et al. 2022; Palmer et al. 2023).

Empirical orthogonal function (EOF; Wilks 2006) analysis was performed on all the observational datasets to identify the leading modes of weekly rainfall variability in the Eastern Africa domain (Fig. 1). The EOF analysis used GPCP and TRMM data with masking over oceanic regions to consider all datasets with land-only grid point information. The eigenvalues and eigenvectors of an anomaly covariance matrix of a field were computed to extract the EOF modes. Since the EOF analysis does not consist of physical assumptions, a field is separated into mathematically orthogonal modes, which occasionally can be translated into physical structures (Hannachi et al. 2007). The eigenvalues are used to express the percentage of variance explained by each EOF mode. Nevertheless, the eigenvalues may not always be distinguishable owing to sampling issues. The North's rule of thumb was used to overcome this constraint by evaluating if a particular eigenvalue is distinct from its nearest neighbour and indicating when a sampling error is expected to be significant (North et al. 1982). Rainfall anomalies were projected onto the generated eigenvectors to produce normalised time series, or principal components (PCs), associated with each EOF mode.

To investigate possible associations between the dominant modes of weekly Eastern Africa short rains variability and potential drivers of sub-seasonal rainfall variations, we calculated climate indices frequently used as indicators of MJO, ENSO, and IOD activity. These are the RMM daily index (Wheeler and Hendon 2004), the Niño 3.4 (hereafter referred to as N3.4) index (Trenberth and

UNCORRECTED PROOF



Journal : Large 382 | Article No : 7244 | Pages : 17 | MS Code : 7244 | Dispatch : 19-4-2024

Stepaniak 2001) and the Dipole Mode Index (DMI; Saji et al. 1999), respectively.

The European Centre for Medium-Range Weather Forecasts (ECMWF) data store provided the RMM components (i.e., RMM1 and RMM2) calculated as in (Vitart 2017). The RMM components illustrate different phases of the MJO cycle (Wheeler and Hendon 2004), with RMM1 (RMM2) representing MJO convective anomalies over the Maritime Continent and Western Hemisphere (tropical Indian Ocean and western Pacific). These indices are the two leading PCs extracted from an EOF analysis, which combines daily zonal upper- (200 hPa) and lower- (850 hPa) wind and outgoing long-wave radiation anomalies in the tropics after subtracting the low-frequency variability associated with ENSO (as in Wheeler and Hendon 2004). Weekly RMM components were determined using the same approach applied to obtain weekly rainfall totals. SST anomalies in the N3.4 region (5°S–5°N, 120°–170°W) were averaged to produce the N3.4 index, whereas the DMI index was determined by the difference between SST anomalies in the western (10°S–10°N, 50°–70°E) and eastern (10°S–0°, 90°–110°E) tropical Indian Ocean. SST data were sourced from the daily optimum interpolation SST version 2 of the National Oceanic and Atmospheric Administration (NOAA; Reynolds et al. 2007). The same technique applied to find weekly rainfall anomalies was employed to obtain weekly SST anomalies, which were used to calculate N3.4 and DMI indices. The respective standard deviations were utilised to normalise weekly SST anomaly indices. Additionally, considering that ENSO and IOD may have strong associations during the boreal autumn (Nicholson 2015; Zhang et al. 2015), we removed from N3.4 and DMI indices their variability associated with DMI and N3.4 indices (hereafter referred to as N3.4* and DMI* indices), respectively. This was performed by first computing a simple linear regression (Allen 1997) between the response and explanatory variables, then subtracting the corresponding co-variability from N3.4 and DMI indices.

Pearson's correlation (Wilks 2006) was computed to indicate linear associations between the leading TAMSAT PCs and drivers' indices, in addition to showing the strength of the linear relationship between the PCs derived from observational datasets. The magnitude of the correlation was determined by its absolute value (or modulus). Therefore, the higher the absolute correlation, the stronger the association. A two-sided Student's t-test with a 95% significance level was used to examine the statistical robustness of correlations distinct from zero (Wilks 2006). Based on lag-1 autocorrelation, the effective sample size was estimated as in Livezey and Chen (1983).

## 2.2 Hindcast assessment

The ability of dynamical models to capture and predict the leading modes of sub-seasonal Eastern Africa short rains variability was evaluated using hindcasts from ECMWF, the National Centers for Environmental Prediction (NCEP), and the UK Met Office (UKMO) models. Using these models allows us, in particular, to expand the hindcast assessment conducted by de Andrade et al. (2021), contributing to enhancing the knowledge of sub-seasonal rainfall forecast quality in Eastern Africa. Rainfall hindcasts were obtained from two sub-seasonal forecasting databases: the Subseasonal to Seasonal (S2S) prediction project (Vitart et al. 2017) for ECMWF and UKMO models, and the Subseasonal Experiment (SubX; Pegion et al. 2019) for the NCEP model. The SubX database was used for NCEP to allow a longer time frame (i.e., 1999–2016) than what is provided in the S2S database (i.e., 1999–2010). ECMWF and UKMO hindcasts were sourced at the regular 1.5° × 1.5° spatial resolution, whereas the NCEP grid was reduced from 1° × 1° to 1.5° × 1.5° using bi-linear interpolation. As in de Andrade et al. (2021), four start dates per month, based on weekly UKMO initialisations, were evaluated for each model, accounting for the closest start dates for some non-matching ECMWF initialisations. Moreover, three perturbed members, drawn from 1-day lag after initialisations, were added to the NCEP ensemble size to achieve an accurate intercomparison between models while considering the same ensemble size (i.e., at least 7 ensemble members). The amount of weekly rainfall was defined by averaging the following daily forecast lead times falling within the short rains season: days 5–11 (Week 1), 12–18 (Week 2), 19–25 (Week 3), and 26–32 (Week 4). This implied that a few initialisations in September and December were respectively included and removed when evaluating targets at Weeks 2–4 leads. The ensemble mean climatology, calculated considering a leave-one-out cross-validation approach (Wilks 2006), was subtracted from the ensemble mean totals to obtain the corresponding anomalies over the 1999–2016 period. The procedure was carried out depending on the start date and lead time. An equivalent method was used to determine observed rainfall anomalies in Weeks 1–4.

The leading PCs of modelled rainfall variability at Weeks 1–4 were calculated by projecting land-only model anomalies onto the observed rainfall eigenvectors determined in Section. 2.1 By regressing the derived PCs and model anomalies, it yielded the corresponding modelled regressed spatial modes (RSMs). Observed PCs and associated RSMs at Weeks 1–4 were obtained considering the same approach used to identify the dominant rainfall modes within models. To extract modelled and observed spatiotemporal modes



Journal : Large 382 | Article No : 7244 | Pages : 17 | MS Code : 7244 | Dispatch : 19-4-2024

UNCORRECTED PROOF

for each lead time, we utilised samples with 180 (i.e., 10 start dates over 18 years) weekly hindcast and observation anomalies, respectively.

The ability of the model to capture the RSMs was evaluated by computing spatial correlation (i.e., Pearson's correlation was examined in two spatial dimensions considering an area-average weighted with latitude) and the region-averaged absolute difference (or modulus of the difference) between modelled and observed RSMs. Additionally, the ability of the model to predict the PCs was assessed by computing Pearson's correlation and root mean squared error (RMSE; Wilks 2006) between modelled and observed PCs. Correlations were computed to assess model phase errors, with values equal to one indicating the strongest linear associations between observations and model data. On the other hand, model amplitude errors were assessed using RMSE and absolute difference, with values equal to zero indicating the best model accuracy. The statistical significance of the correlations was examined as described in Section 2.1.

### 2.3 Drivers of model skill

The contribution of climate drivers in modulating the ECMWF model skill at predicting the main modes of weekly Eastern Africa short rains variability was investigated employing a similar methodology as the one described in de Andrade et al. (2021). The method assesses the ECMWF model skill after replacing the modelled driver-related rainfall variability with the corresponding observed driver-related response in the hindcasts. Observed and modelled driver-related rainfall variabilities are derived from the corresponding linear regression between rainfall anomalies and climate indices representing MJO, ENSO, and IOD variations. Here, RMM, N3.4, and DMI indices were respectively used to characterise MJO, ENSO, and IOD activity as in de Andrade et al. (2021). Daily RMM components for each model ensemble member were sourced from the ECMWF data store, allowing the computation of the 7-member ensemble mean for RMM1 and RMM2 indices at Weeks 1–4. Furthermore, daily SST hindcasts from the S2S database were used to obtain the 7-member ensemble mean of weekly SST anomalies, following the procedures adopted to obtain weekly rainfall anomalies in Section 2.2. ENSO and IOD indices at Weeks 1–4 were computed as in Sect. 2.1, with their co-variability also removed from modelled N3.4 and DMI for producing modelled N3.4* and DMI* indices. Both indices were normalised by the corresponding standard deviation depending on the initialisation and lead time. Suitable datasets specified in Sect. 2.1 were used to produce the observed RMM1, RMM2, N3.4*, and DMI* indices in Weeks 1–4.

Next, we performed a simple linear regression analysis between weekly rainfall anomalies and MJO, ENSO, and IOD indices. We subtracted from both observed and modelled rainfall anomalies the corresponding variations in rainfall that were linearly associated with each driver. Rainfall anomalies without the presence of drivers' signals were used to calculate observed and modelled PCs at Weeks 1–4 as in Section 2.2. After removing driver-related rainfall variability from modelled rainfall anomalies, the impact on the model skill was also investigated by adding observed regression patterns to hindcasts, producing a new set of model rainfall anomalies utilised to obtain corrected PCs. The model skill was evaluated by measuring the percentage change in Pearson's correlation between the resulting observed and modelled PCs according to (1):

$$((\widehat{R} - R)/R) * 100 \quad (1)$$

Where R is the correlation computed without modifying any driver-related signals in rainfall anomalies, and $\widehat{R}$ is the correlation after removing or adding particular driver-related signals in rainfall anomalies. Positive (Negative) values of (1) denote strengthening (weakening) in the association between observed and modelled PCs, indicating, therefore, improvements (degradations) in the model skill.

## 3 Results

The results are organised into three sections, which systematically respond to the questions presented in Section 1. The first Section (3.1) identifies and compares the leading modes of sub-seasonal Eastern Africa short rains variability from distinct observational datasets, and shows how these modes relate to specific climate drivers. The second Section (3.2) presents a hindcast evaluation for investigating the ability of the model to capture and predict the leading rainfall modes at forecast horizons from one to four weeks into the future. The third Section. (3.3) furthers this evaluation to consider how the model quality is related to the potential sources of sub-seasonal climate variability.

### 3.1 The leading EOF modes and their associations with climate drivers

Figure 2 shows weekly TAMSAT rainfall climatology, the standard deviation of associated anomalies, and the corresponding EOF analysis for Eastern Africa rainfall anomalies during the short rains season from October to December. The highest climatological rainfall totals are located over elevated topography in the western sector of Eastern Africa, covering parts of Burundi, Rwanda, South Sudan, Tanzania, Uganda, and the central-eastern Democratic Republic of the Congo (DRC; Figs. 1, 2a). In contrast, the highest rainfall variability appears in the southeastern sector of Eastern

UNCORRECTED PROOF



Journal : Large 382 | Article No : 7244 | Pages : 17 | MS Code : 7244 | Dispatch : 19-4-2024

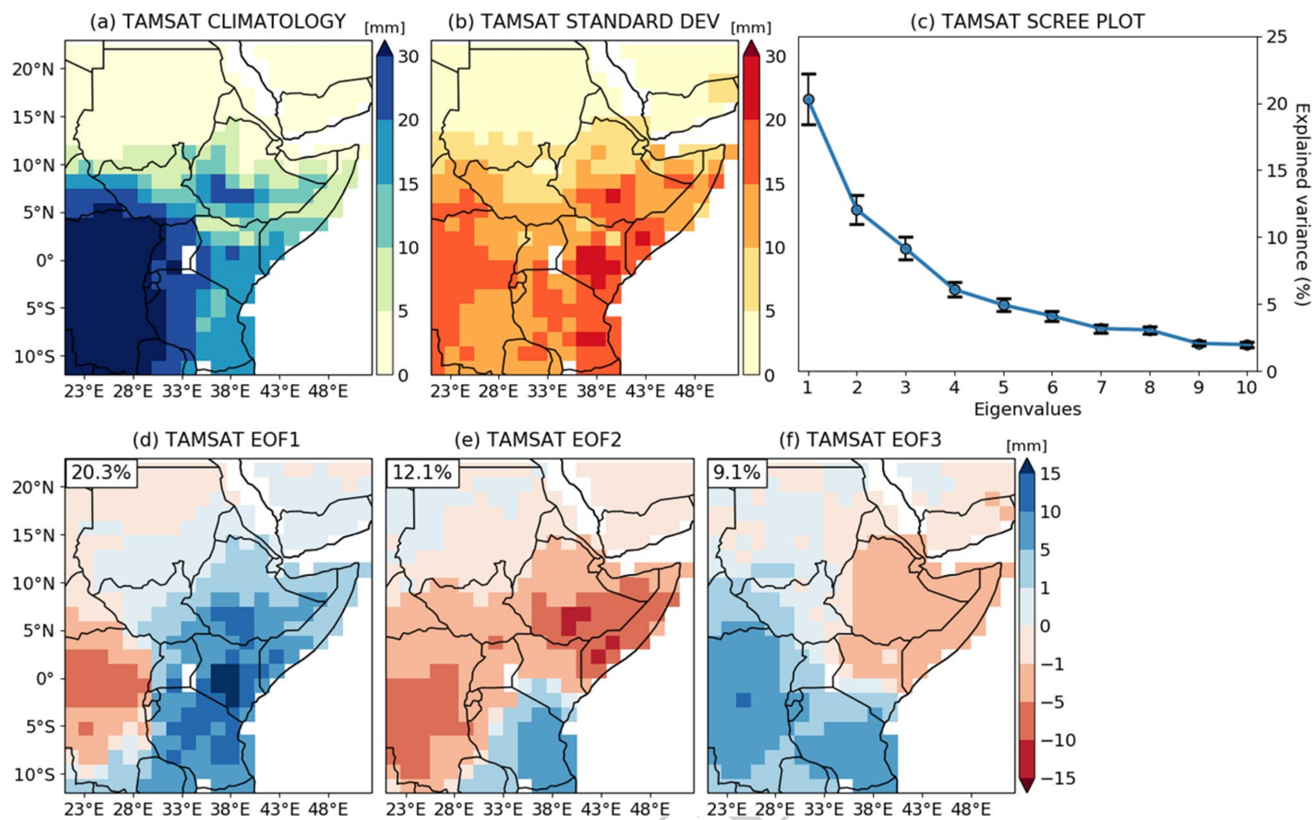


**Fig. 2** Weekly TAMSAT accumulated rainfall (a) climatology and (b) standard deviation for Eastern Africa short rains season (OND). (c) Scree plot showing the corresponding explained variance in percentage (%) for the first ten eigenvalues of the EOF analysis from weekly TAMSAT rainfall anomalies. Sample errors are indicated by the error bars in (c) according to the North's rule of thumb. The first three spatial EOF modes (or eigenvectors) for weekly TAMSAT rainfall accumulation anomalies are respectively displayed in (d), (e), and (f), with their explained variance in percentage (%) shown in the top-left corner. Rainfall accumulations are in millimetres (mm)

Africa, including the highlands of Ethiopia and Kenya, as well as coastal regions in Somalia and Tanzania (Figs. 1, 2b). The first three EOF modes for TAMSAT show spatial structures that influence varying rainfall levels in most Eastern Africa countries and, when combined, account for 41.5% of the total variance (Figs. 2d, e, f). According to the criteria of North et al. (1982), these dominant modes are distinguished from each other and well separated from the degenerate set of higher EOFs (Fig. 2c).

The first leading mode (EOF1) is characterised by a monopole-like rainfall pattern with the largest positive rainfall anomalies affecting southern Ethiopia, Kenya, and northern Tanzania (Fig. 2d). The second (EOF2) and the third (EOF3) modes show a dipole-like rainfall pattern with positive anomalies in Tanzania and negative anomalies in the northeastern portion of Eastern Africa, which covers Djibouti, Eritrea, Ethiopia, and Somalia (Figs. 2e, f). EOF2 and EOF3 have similar spatial characteristics in the eastern part of the domain and coastal regions, whereas opposite signals are seen further inland (Figs. 2e, f). Although using other datasets, periods, and domains, the EOF modes found here generally correspond well with the main modes of seasonal and pentad Eastern Africa rainfall variability identified in previous studies (Schreck and Semazzi 2004; Bowden and Semazzi 2007; Wenhaji Ndomeni et al. 2018; Kolstad and MacLeod 2022).

To investigate sources of sub-seasonal Eastern Africa short rains variability, Fig. 3 presents the correlations between potential climate drivers' indices and the first three TAMSAT PCs. RMM1 exhibits strong significant connections with PC2 and PC3, whereas.

RMM2 shows high significant co-variability linked to PC1 (Fig. 3a). Despite N3.4 and DMI showing significant correlations with PC1, as also found in previous studies (Schreck and Semazzi 2004; Bowden and Semazzi 2007; Kolstad and MacLeod 2022), it is worth pointing out that for N3.4, removing the signal associated with DMI makes the association insignificant (compare the correlations when considering the ENSO index as N3.4 (darkest blue bar) and N3.4* (lightest blue bar) in Fig. 3a), whereas removing the N3.4 signal from DMI does weaken the correlation with PC1 but it is still significant (compare the correlations when considering the DMI index as DMI (darkest red bar) and DMI* (lightest red bar) in Fig. 3a).



Journal : Large 382 | Article No : 7244 | Pages : 17 | MS Code : 7244 | Dispatch : 19-4-2024

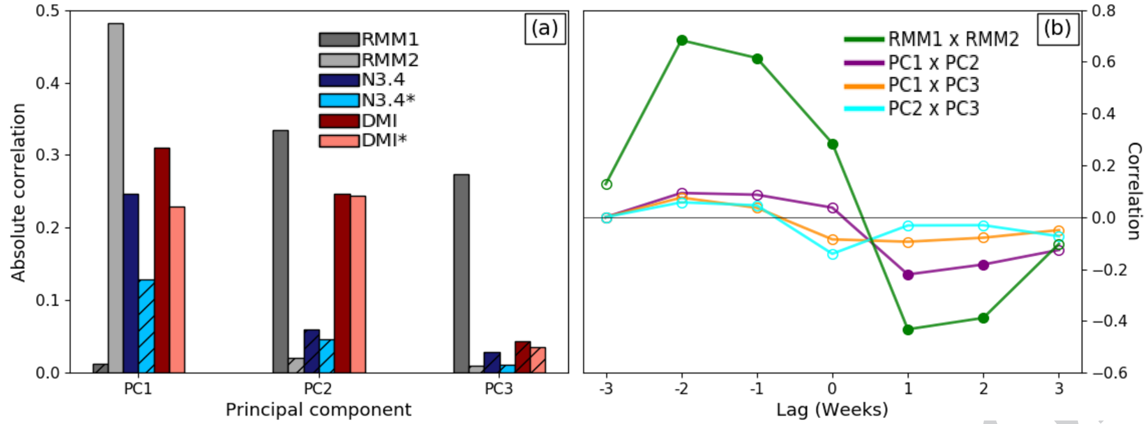


**Fig. 3** (a) Absolute Pearson's correlation between weekly TAMSAT PC1 to PC3 and observed weekly drivers' indices represented by RMM1, RMM2, N3.4, and DMI. N3.4* (DMI*) indicates that the DMI (N3.4) signal has been removed from the N3.4 (DMI) index. (b) Lagged correlations between RMM1 and RMM2, as well as between the leading TAMSAT PCs. A positive (negative) lag indicates RMM1 leads (lags) RMM2, for instance. Hatching over the bars in (a) and open circle markers in (b) denote correlation coefficients that are not statistically significant at the 95% confidence level according to a two-tailed Student's t-test

For PC2, the correlations indicate that the MJO and IOD have significant associations with the dipole-like rainfall variability in the region. In contrast, there are no significant associations between ENSO and PC2 (Fig. 3a). Unlike PC1 and PC2, PC3 does not significantly correlate with SST indices, which mainly emphasises its relationship with the MJO (Fig. 3a).

The climate drivers' associations with TAMSAT PC1 and PC2 (Fig. 3a), along with the corresponding TAMSAT spatial modes shown in Fig. 2, generally are consistent with the regression patterns that de Andrade et al. (2021) found when relating similar drivers' indices to weekly GPCP rainfall anomalies. That is, EOF1 (Fig. 2d) compares quite strongly to the September–October-November RMM2- and DMI-related rainfall patterns shown in de Andrade et al. (2021) (see SON in their Fig. 9), whereas EOF2 (Fig. 2e) reasonably matches with the corresponding SON RMM1-related rainfall pattern. Moreover, December-January–February N3.4- and RMM1-related rainfall patterns shown in de Andrade et al. (2021) (see DJF in their Fig. 9) also indicate consistent signals with TAMSAT EOF1 (Fig. 2d) and EOF2 (Fig. 2e), respectively. All these characteristics corroborate with GPCP EOF1 and EOF2, as shown later in Fig. 5.

To specifically deepen understanding of the MJO-related Eastern Africa rainfall variability, Fig. 3b shows the lagged correlation between RMM components, as well as between TAMSAT PC1, PC2, and PC3. Significant correlations for PC1 and PC2 are identified at 1–2-week lags, showing that PC1 generally leads PC2 by a few weeks (Fig. 3b; purple line). This agrees with the MJO cycle, which also indicates that RMM1 and RMM2 occur sequentially with significant correlations at 1–2-week lags (Fig. 3b; green line). However, the correlations between PC1 and PC3 or PC2 and PC3 are not significant across all lags (Fig. 3b; orange and blue lines).

The results discussed so far have been carried out using TAMSAT data. To examine the sensitivity of weekly rainfall to the choice of the observational dataset, Fig. 4 displays the climatology and standard deviation for CHIRPS (Figs. 4a, d), GPCP (Figs. 4b, e), and TRMM (Figs. 4c, f) data during OND.

All datasets show the highest climatological rainfall totals in the western sector of the domain (Figs. 4a, b, c) and the highest rainfall deviations in the southeastern sector of Eastern Africa (Figs. 4d, e, f), overall corroborating with TAMSAT data (Figs. 2a, b). Nevertheless, higher (lower) climatological rainfall totals are seen over Kenya for CHIRPS and TRMM (GPCP) data (compare Fig. 2a with Figs. 4a, c (Fig. 4b)), whereas higher (lower) rainfall variations are found further inland for GPCP and TRMM (CHIRPS) data (compare Fig. 2b with Figs. 4e, f (Fig. 4d)). Despite these minor differences in the rainfall data, there is considerable agreement in the weekly evolution of the region-averaged rainfall anomalies throughout the short rains when comparing all datasets (Online Resource 1—Fig. 1). These findings, therefore, contribute to increasing the reliability of the observed rainfall variability in the region and its related EOF analysis, as shown below.

Figure 5 displays the first three spatial EOF modes and scree plots for CHIRPS, GPCP, and TRMM rainfall anomalies. The combined explained variance of EOF1, EOF2, and EOF3 is 42.1% for CHIRPS (Figs. 5a, b, c), 45.4% for GPCP (Figs. 5e, f, g), and 34.4% for TRMM (Figs. 5i, j, k). Thus, the sum of the explained variance of TRMM is lower than that of CHIRPS or GPCP when compared to TAMSAT (41.5%; Figs. 2d, e, f).

UNCORRECTED PROOF



Journal : Large 382 | Article No : 7244 | Pages : 17 | MS Code : 7244 | Dispatch : 19-4-2024

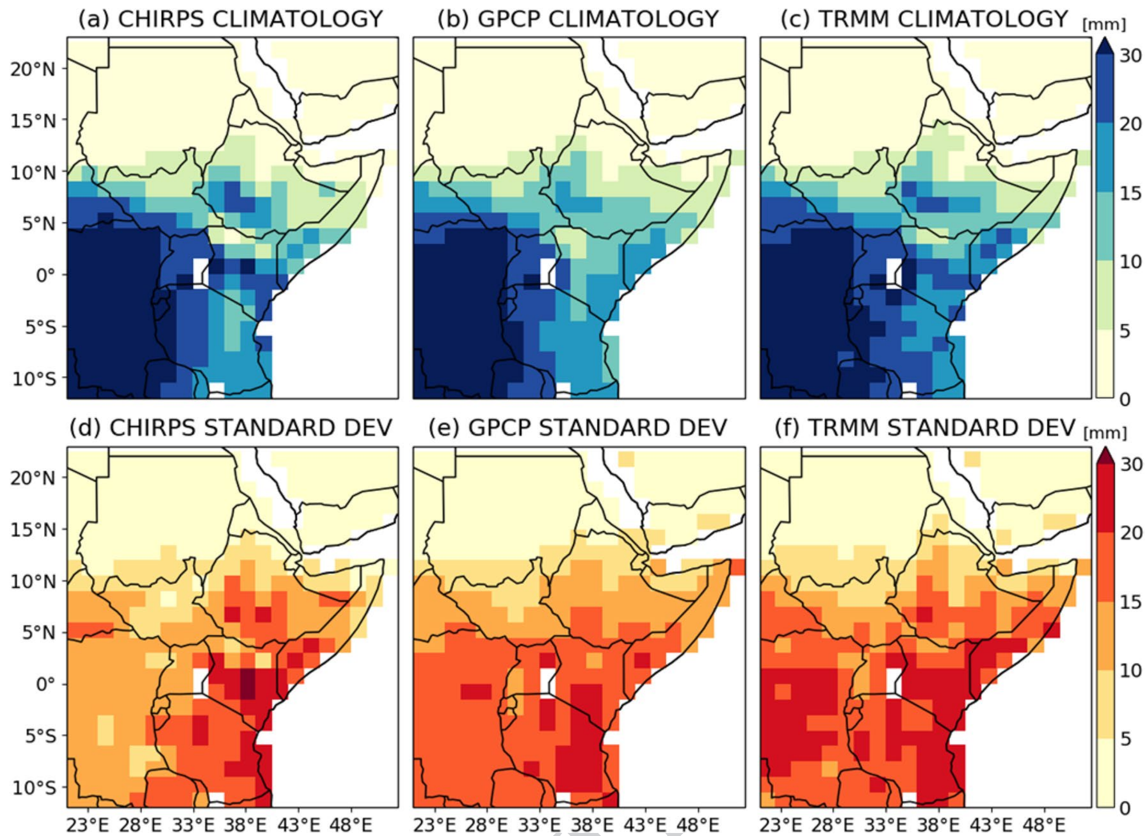


**Fig. 4** Weekly accumulated rainfall (upper panel) climatology and (lower panel) standard deviation for (a, d) CHIRPS, (b, e) GPCP, and (c, f) TRMM datasets during the Eastern Africa short rains season (OND). Rainfall accumulations are in millimetres (mm)

The spatial patterns associated with EOF1 and EOF2 from the additional datasets (CHIRPS, GPCP, and TRMM) are similar to the ones found for TAMSAT, i.e., a monopole-like rainfall pattern for EOF1 (compare Fig. 2d with Figs. 5a, e, i) and a dipole-like rainfall pattern for EOF2 (compare Fig. 2e with Figs. 5b, f, j). For EOF3, however, there are discrepancies when comparing its spatial pattern among the datasets. While GPCP shows positive rainfall anomalies in Tanzania and negative rainfall anomalies in the northeastern sector of Eastern Africa in agreement with TAMSAT (compare Fig. 2f with Fig. 5g), CHIRPS and TRMM exhibit rainfall patterns that differ from TAMSAT (compare Fig. 2f with Figs. 5c, k). The uncertainty in representing EOF3 in the observations is also seen through the scree plots, showing distinct sample errors and how separated this mode is from EOF2 and higher EOF modes, depending on the dataset (Figs. 5d, h, l).

To further assess the representation of the leading EOF modes within CHIRPS, GPCP, and TRMM datasets, Fig. 6 shows the association between the first three TAMSAT PCs and the first ten PCs (PC1 to PC10) derived from the EOF analysis using CHIRPS, GPCP, and TRMM rainfall anomalies. The highest correlation coefficients indicate that TAMSAT PC1 and PC2 are adequately represented across all datasets, particularly in CHIRPS data (Figs. 6a, b). However, Fig. 6c shows there is some sensitivity to the selection of the reference data when performing an EOF analysis of weekly rainfall anomalies for Eastern Africa short rains, specifically that TAMSAT PC3 properties are not well represented by other datasets, notably CHIRPS and TRMM as also seen in the spatial patterns (compare Fig. 2f with Figs. 5c, k). In fact, CHIRPS can reasonably represent the temporal variability associated with EOF3, though it is captured by the fourth EOF mode (Fig. 6c).

The following two sections only address a model evaluation for the first two EOF modes (EOF1 and EOF2) owing to the inconsistency in representing EOF3 across the datasets (Figs. 2, 5, 6). Moreover, the results for the TAMSAT dataset are exclusively used when assessing model hindcasts, as the sensitivity to the reference data selection is minimal for the two leading rainfall modes (Figs. 2, 5, 6).

### 3.2 Model evaluation

Figures 7 and 8 show the model capability to capture the first (RSM1) and the second (RSM2) RSMs at lead times

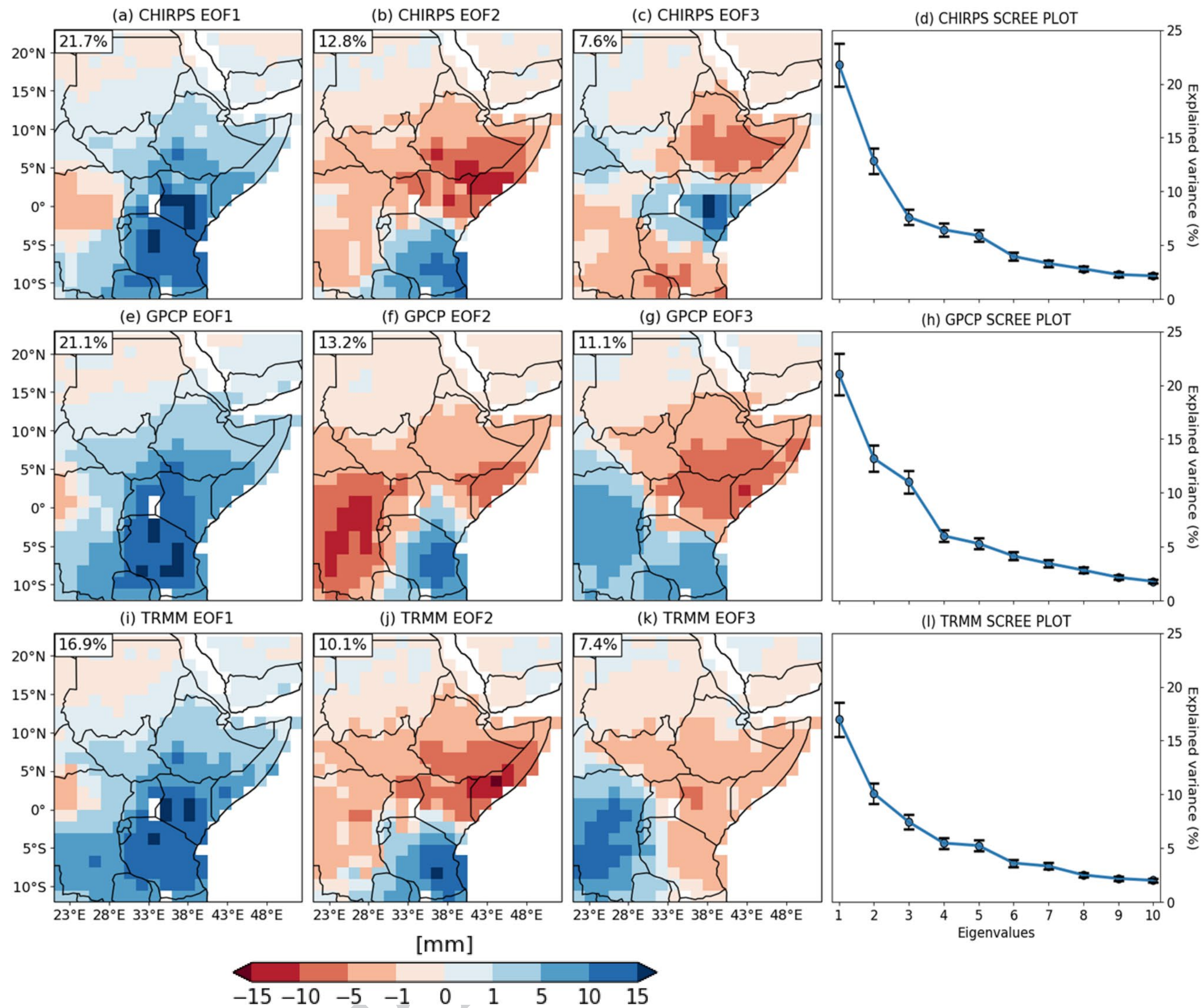


**Fig. 5** The first three spatial EOF modes (or eigenvectors) for weekly (a)-(c) CHIRPS, (e)-(g) GPCP, and (i)-(k) TRMM rainfall accumulation anomalies during OND, with their explained variance in percentage (%) shown in the top-left corner. Scree plot showing the corresponding explained variance in percentage (%) for the first ten eigenvalues of the EOF analysis from weekly (d) CHIRPS, (h) GPCP, and (l) TRMM rainfall anomalies. Sample errors are indicated by the error bars in (d, h, l) according to the North's rule of thumb. Rainfall accumulations are in millimetres (mm)

UNCORR

of one to four weeks ahead, respectively. Even though the amplitude of anomalies reduces with increasing lead time, all models can satisfactorily represent essential characteristics of the leading RSMs, that is, the monopole-like rainfall pattern for RSM1 (Fig. 7) and the dipole-like rainfall pattern for RSM2 (Fig. 8), in agreement with the observations (contours in Figs. 7, 8). The ability of the NCEP model to capture RSM1 and RSM2 is lower than in other models, as indicated by the largest region-averaged amplitude differences and the weakest spatial correlation coefficients computed between modelled and observed RSMs. Less accurate outcomes in the NCEP model are, in particular, associated with errors in representing the location of the rainfall anomaly. For RSM1, this is seen through the largest positive anomalies displaced to the west of Tanzania (Figs. 7e, f, g, h) compared to the ECMWF (Figs. 7a, b, c, d) and UKMO (Figs. 7i, j, k, l) models. ECMWF and UKMO models place such variations in rainfall over the entire southeastern sector of Eastern Africa, as also seen in the observations. For RSM2, the discrepancy is found in the largest negative anomalies (Figs. 8e, f, g, h), which appear further to the west of the domain compared to the other models and observations (Figs. 8a, b, c, d, i, j, k, l).

Shortcomings in capturing the leading RSMs are likely related to the model capability of representing its climatology and variance (Online Resource 1—Figs. 2, 3). Although all models predict the highest climatological rainfall totals in



Journal : Large 382 | Article No : 7244 | Pages : 17 | MS Code : 7244 | Dispatch : 19-4-2024

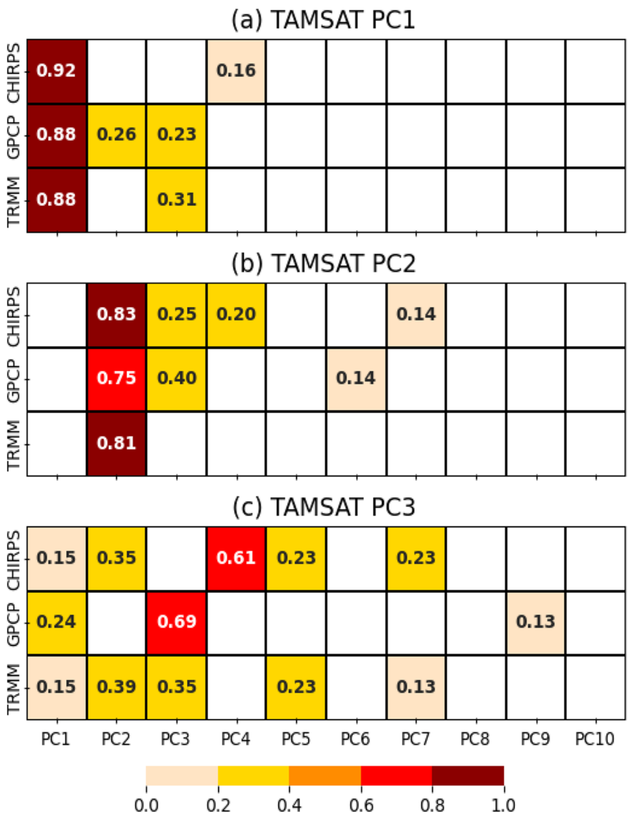


**Fig. 6** Absolute Pearson's correlation for TAMSAT (a) PC1, (b) PC2, and (c) PC3 against the first ten PCs (PC1 to PC10) from CHIRPS, GPCP, and TRMM datasets. Shaded boxes with numbers indicate statistically significant values at the 95% confidence level according to a two-tailed Student's t-test

the western portion of the domain, the mean state response for ECMWF and UKMO (NCEP) is stronger (weaker) than TAMSAT over most of the southern and southeastern sectors of Eastern Africa (compare Fig. 2a with Online Resource 1—Fig. 2). Additionally, all models show a reduction in rainfall variability with increasing lead time, as well as discrepancies at predicting the location of rainfall anomalies, particularly in the NCEP model, which shows higher deviations near DRC compared to TAMSAT (compare Fig. 2b with Online Resource 1—Fig. 3).

The model skill at predicting the leading PCs (PC1 and PC2) in Weeks 1–4 is evaluated in Fig. 9. For both PCs, the skill reduces with increasing lead time, with, in particular, Week 1 showing the highest associations (Fig. 9a) and lowest amplitude errors (Fig. 9b) for all models PC1. UKMO and ECMWF PC1 have the highest skill at all leads, with UKMO having a marginally higher skill than ECMWF. The results for PC1 overall corroborate the correlation assessments performed by de Andrade et al. (2021) for weekly Eastern Africa rainfall anomalies initialised in September–October-November. All models exhibit higher skill at predicting PC1 compared with PC2. Notably, the skill for NCEP PC1 remains just slightly higher than for ECMWF or UKMO PC2 in Weeks 3–4, and even comparable to these models PC2 in Week 2. The lowest skill is seen for NCEP PC2 at most leads, showing, for instance, a non-significant correlation with a value below 0.2 at Week 4 (Fig. 9a).

## 4 Sources of predictability

To investigate where the skill found in the previous section comes from, Figs. 10 and 11 show respectively the percentage change in the correlations for ECMWF PC1 and PC2 against the corresponding observed PCs considering two conditions: i) when the co-variability between modelled rainfall anomalies and specific climate drivers' indices is subtracted from the model (Figs. 10a, 11a) and (ii) when the corresponding observed co-variability is added to the model (Figs. 10b, 11b) after removing its modelled co-variability as in (i). According to Eq. (1), both conditions (i) and (ii) are relative to reference values obtained when no modification is considered in the model rainfall anomalies before computing the PCs. Since ECMWF and UKMO had comparative skill in Fig. 9, with skill significantly higher than NCEP, the former is used here to compare the results with those found in de Andrade et al. (2021).

The driver-rainfall co-variability subtracted from modelled rainfall anomalies modulates the skill at predicting PC1 (Fig. 10a) and PC2 (Fig. 11a) throughout the lead times. When examining the removal of a single driver's signal rather than a combination of two or more of these drivers' signals in the model, the skill degradation (i.e., negative percentage change) for PC1 is mainly seen after removing the RMM2 signal from hindcasts (Fig. 10a). This shows a correlation reduction varying from 9.3% in Week 1 to 53.8% in Week 4 relative to reference values (i.e., CORR in Fig. 10a). Removing N3.4* and DMI* signals from hindcasts also affects the PC1 skill. Nevertheless, the rate of skill degradation over the weeks is no higher than 11.6% for N3.4* and 15.2% for DMI* about reference values (Fig. 10a). For PC2 (Fig. 11a), the highest skill degradations occur when removing RMM1- and DMI*-related rainfall anomalies from hindcasts, with skill reducing over the weeks up to 31.5% and 36.2%, respectively, comparing to reference values (i.e., CORR in Fig. 11a). When all drivers' signals are eliminated from the model, the overall skill drop estimated is substantially explained by skill degradation associated with the removal of the MJO signal from hindcasts (compare RMM2 and RMM1 with ALL in Figs. 10a and 11a, respectively), which is more pronounced for PC1 than for PC2 (compare RMM2 in Fig. 10a with RMM1 in Fig. 11a). These decreases in skill seen when subtracting all drivers' signals from hindcasts are also considerably associated with removing the DMI* signal in the model, particularly for PC2

UNCORRECTED PROOF

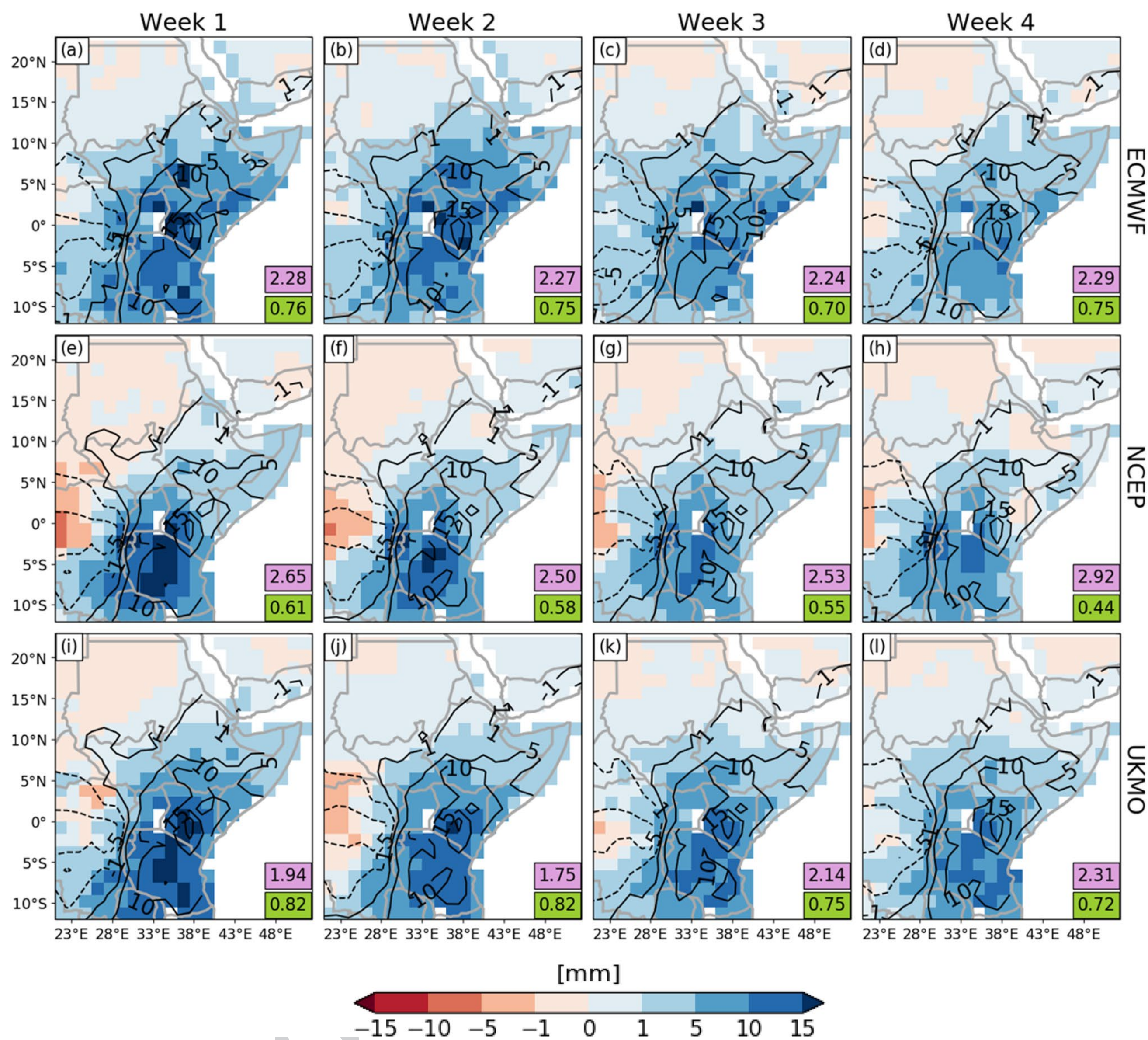


**Fig. 7** First regressed spatial mode (RSM1) at Weeks 1–4 for (a)-(d) ECMWF, (e)-(h) NCEP, and (i)-(l) UKMO models (shaded). The contours denote the corresponding RSM for TAMSAT rainfall anomalies, with solid (dashed) lines for positive (negative) values. The zero line is omitted. Magenta (Green) boxes in the bottom-right corner indicate the region-averaged absolute difference (statistically significant spatial correlation) between modelled and observed RSMs. Statistically significant spatial correlation at the 95% level confidence level is examined according to a two-tailed Student's t-test

(compare DMI* with ALL in Figs. 10a, 11a). The combined removal of rainfall variations linked to RMM components (RMM1 + RMM2) and SST indices (N3.4* + DMI*) further indicates that degradations in PC1 forecast skill are mainly related to the RMM2 signal, and are secondarily associated with N3.4* and DMI* signals (Fig. 10a). For PC2, however, such a combined removal affecting its prediction skill is dominated by RMM1 and DMI signals in the model (Fig. 11a). Thus, these forecast skill results for PC1 and PC2 corroborate the corresponding observed associations shown in Fig. 3.

Skill improvements (i.e., positive percentage changes) are seen for both PC1 and PC2 predictions after replacing the modelled rainfall response to a single driver with the corresponding observed response, especially in Weeks 3–4 (Figs. 10b, 11b). Although PC1 and PC2 skills improve if using corrected DMI*-related rainfall variability patterns, this approach is not more effective than simply correcting the model with the observed MJO-related rainfall variability. Moreover, the effect of adjusting the rainfall signal associated with N3.4* in the model is almost zero (Figs. 10b, 11b), indicating that of



| Journal : Large 382 | Article No : 7244 | Pages : 17 | MS Code : 7244 | Dispatch : 19-4-2024 |
| --- | --- | --- | --- | --- |

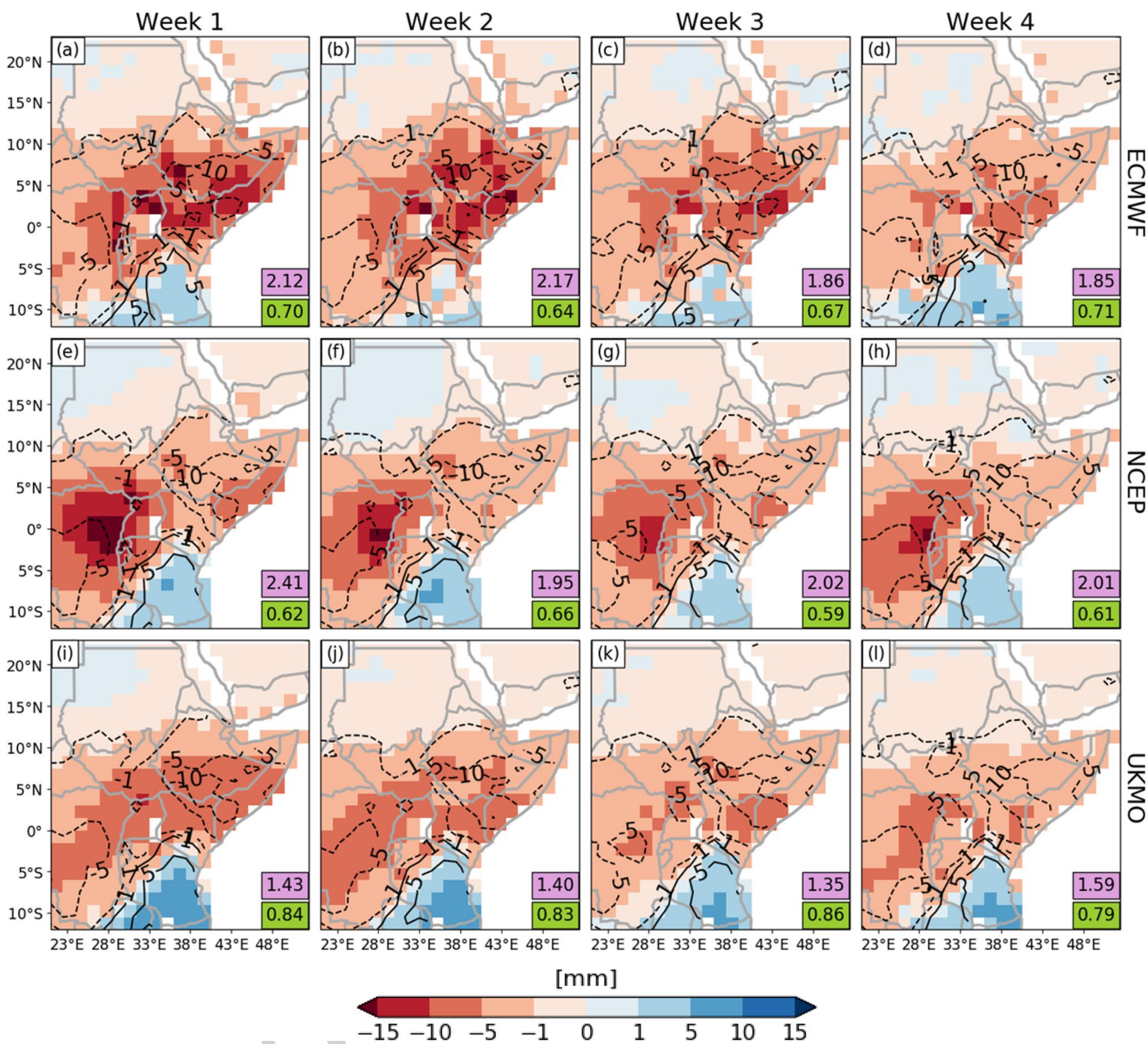


**Fig. 8** Second regressed spatial mode (RSM2) at Weeks 1–4 for (a)-(d) ECMWF, (e)-(h) NCEP, and (i)-(l) UKMO models (shaded). The contours denote the corresponding RSM for TAMSAT rainfall anomalies, with solid (dashed) lines for positive (negative) values. The zero line is omitted. Magenta (Green) boxes in the bottom-right corner indicate the region-averaged absolute difference (statistically significant spatial correlation) between modelled and observed RSMs. Statistically significant spatial correlation at the 95% level confidence level is examined according to a two-tailed Student's t-test

the predictability drivers investigated here, ENSO contributes the least to varying PCs forecast skill. PC1 skill improvements are more sensitive to RMM2 variations than to anomalies in other drivers (Fig. 10b), whereas the most pronounced PC2 skill responses are linked to RMM1 variations (Fig. 11b). These findings are supported, for example, by the largest positive percentage changes for PC1 and PC2 in Week 4, with correlation coefficients exceeding, respectively, 50% (RMM2 in Fig. 10b) and 70% (RMM1 in Fig. 11b) relative to reference values (i.e., CORR in Figs. 10b, 11b). For PC2 rather than PC1, skill improvements associated with MJO are more pronounced (compare RMM1 in Fig. 11b with RMM2 in Fig. 10b), and account for a considerable portion of the enhanced overall level of skill after including all observed drivers' signals in the model (compare RMM1 and RMM2 with ALL in Figs. 11b and 10b, respectively).

The results presented in this section overall corroborate the ones found by de Andrade et al. (2021), highlighting, in particular, the potential contribution of improved

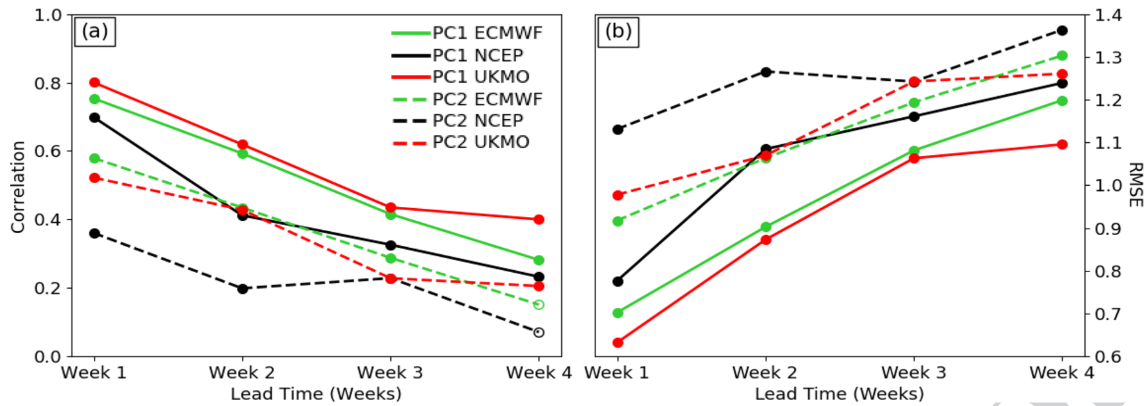


**Fig. 9** (a) Correlation and (b) RMSE for the first two observed (TAMSAT) and modelled (ECMWF, NCEP, and UKMO) PCs (PC1 and PC2) at Weeks 1–4. Solid (Dashed) lines indicate the skill assessment for PC1 (PC2). The open circle marker in (a) denotes correlation coefficients that are not statistically significant at the 95% level confidence level according to a two-tailed Student's t-test

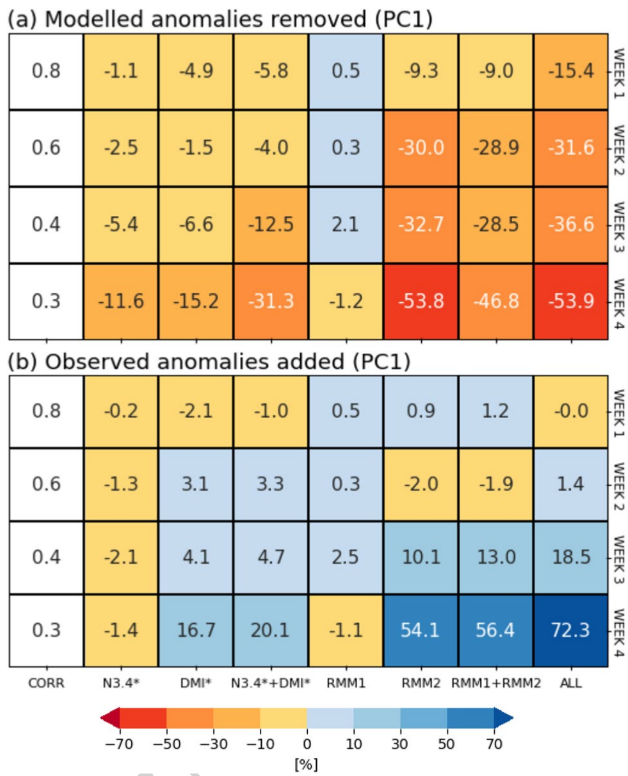


**Fig. 10** Percentage change in the correlation between TAMSAT and ECMWF PC1 at Weeks 1–4 computed after (a) removing from and (b) adding to model rainfall anomalies a particular driver-related variability. The co-variability is indicated at the bottom of (b) by the corresponding driver's index or a combination of two or all ("ALL") drivers' indices. The leftmost column shows the correlation computed without modifying any driver-related signal in rainfall anomalies ("CORR"), as in Fig. 9a (solid green line)

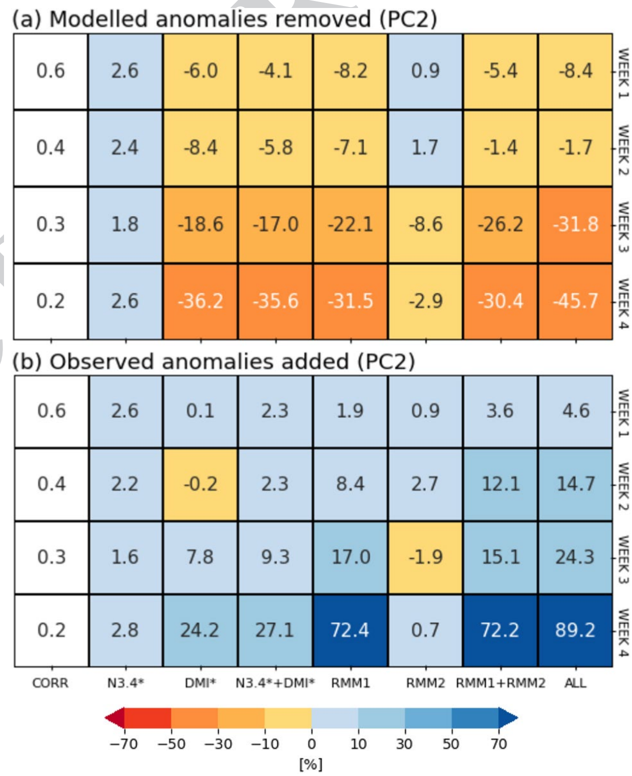


**Fig. 11** Percentage change in the correlation between TAMSAT and ECMWF PC2 at Weeks 1–4 computed after (a) removing from and (b) adding to model rainfall anomalies a particular driver-related variability. The co-variability is indicated at the bottom of (b) by the corresponding driver's index or a combination of two or all ("ALL") drivers' indices. The leftmost column shows the correlation computed without modifying any driver-related signal in rainfall anomalies ("CORR"), as in Fig. 9a (dashed green line)

MJO-related rainfall variability (or a bias correction based on the MJO impacts on model rainfall anomalies) to skill increases in weekly Eastern Africa rainfall predictions within the ECMWF model.



| Journal : Large 382 | Article No : 7244 | Pages : 17 | MS Code : 7244 | Dispatch : 19-4-2024 |
|---|---|---|---|---|

## 5 Summary and conclusions

The sub-seasonal variability and prediction skill of short rains in Eastern Africa are assessed using several observational and model datasets. An EOF analysis is performed to identify the leading modes of weekly rainfall variability in Eastern Africa, allowing exploring their associations with specific climate drivers. This study then goes on to investigate the ability of dynamical models to capture and predict the leading rainfall modes, as well as examine potential-related sources of predictability.

Irrespective of the observational dataset used (i.e., TAMSAT, CHIRPS, GPCP, or TRMM), two distinct weekly rainfall modes in the Eastern African short rains from October to December (OND) are identified; these are: i) a monopole-like rainfall pattern with the largest anomalies in southern Ethiopia, Kenya, and northern Tanzania; and (ii) a dipole-like rainfall pattern between Tanzania and the northeastern sector of Eastern Africa, mainly impacting Ethiopia and Somalia. Our results indicated that the two leading rainfall modes have the strongest correlations with the MJO. Specifically, the first (second) rainfall mode showed the highest correlations with the RMM2 (RMM1) index, which is linked to MJO-related convective anomalies in the tropical Indian Ocean and western Pacific (Maritime Continent and Western Hemisphere). Moreover, we found that the first and second leading modes are significantly correlated with the DMI index, with the former also having significant associations with the N3.4 index if the ENSO-IOD co-variability is retained in the index. Despite using distinct datasets, periods, domains, and methods for representing ENSO and IOD activities, our results complement previous work (e.g., Bowden and Semazzi 2007), suggesting that the modulation of the leading weekly rainfall modes may depend on the MJO variability superimposed on distinct lower-frequency background conditions, which deserves additional investigation.

The ability of ECMWF, NCEP, and UKMO models to capture and predict the two leading rainfall modes at lead times of one to four weeks is also examined. Evaluation of modelled spatiotemporal properties of rainfall modes showed that ECMWF and UKMO are comparable and outperformed NCEP. NCEP exhibited, with respect to observations, a westward shift in the anomalies of both spatial modes, which may explain the model shortcomings in capturing the rainfall associated with those modes. The skill assessments for predicting the corresponding PCs further demonstrated that models' phase and amplitude errors increased from Week 1 to Week 4, with ECMWF and UKMO PC1 having the highest skill at all lead times and PC2 showing lower skill than PC1 for all models.

To improve the understanding of potential sources driving ECMWF model skill, an examination of specific climate drivers in modulating the model ability to predict the leading rainfall modes is further carried out. We showed evidence that if the modelled MJO-related rainfall variability is removed from the model, this leads to a degradation in predicting the leading PCs, with rainfall variations linked to the RMM2 (RMM1) index contributing the most to the percentage change in the PC1- (PC2-) related skill. We also found that removing SST-related rainfall variations in the model modulates skill reductions in both PCs, with ENSO and IOD (IOD) impacting the skill at predicting PC1 (PC2). Skill degradations are mainly compensated after replacing the modelled MJO-related rainfall variability with observed MJO-related rainfall variability in the model, leading to the largest skill improvements in Weeks 3–4. It is worth noting that the skill for PC1 and PC2 is respectively improved by up to 18.2% and 16.8% over the weeks when considering the combination of all corrected driver-related rainfall variability relative to considering the most correlated MJO signal only (i.e., RMM2 for PC1 and RMM1 for PC2). Thus, our results indicate that correcting SST-related rainfall variations in the model, especially those associated with IOD, could have contributed to enhancing the skill in predicting the leading rainfall modes, though suggesting a secondary role.

Even though it is still challenging to predict sub-seasonal variations in Eastern Africa short rains (de Andrade et al. 2021; Kolstad et al. 2021), this study demonstrated, in particular, that strengthening the model ability to capture MJO-related rainfall variability has the potential to more accurately predict the main modes of weekly rainfall variability in the region. These results support the concept of windows of opportunity (Mariotti et al. 2020) that may help forecasters identify periods when sub-seasonal rainfall prediction accuracy is at its highest during Eastern Africa short rains. Additionally, given that the drivers examined interact with each other (e.g., Hendon et al. 2007; Wilson et al. 2013; Zhang et al. 2015) and that their combined activity may impact the rainfall in Eastern Africa during the short rains (e.g., Vashisht and Zaitchik 2022), future work is recommended to specifically elucidate the multi-way interactions among ENSO, IOD, and the MJO, as well as the corresponding effects on the sub-seasonal Eastern Africa short rains prediction skill. However, when examining forecast skill, the limited length of typical hindcast datasets can limit the number of samples of each combination of phases of multiple drivers.

Finally, by projecting sub-seasonal rainfall anomaly forecasts onto the two observed leading rainfall modes examined here, a pair of sub-seasonal rainfall monitoring indices could be used as a forecasting tool in operational routines across Eastern Africa. Therefore, in addition to supporting model

UNCORRECTED PROOF



Journal : Large 382 | Article No : 7244 | Pages : 17 | MS Code : 7244 | Dispatch : 19-4-2024

developers in identifying shortcomings in Eastern Africa rainfall predictions for advancing the sub-seasonal prediction systems in the future, our results can further contribute to developing sub-seasonal forecast products that may add valuable climate information for anticipatory planning decisions across several sectors, such as agriculture, food security, and energy.

**Acknowledgements** We thank TAMSAT, The Climate Hazards Center, the National Center for Atmospheric Research, the National Aeronautics and Space Administration, the International Research Institute for Climate and Society, ECMWF, and NOAA for data provision. This work is based on S2S data. S2S is a joint initiative of the World Weather Research Programme (WWRP) and the World Climate Research Programme (WCRP). The original S2S database is hosted at ECMWF as an extension of the TIGGE database.

**Author contributions** All authors contributed to the study conception, design, and analysis. Material preparation and data collection were performed by Felipe Marques de Andrade. The first draft of the manuscript was written by Felipe Marques de Andrade and all authors commented on previous versions of the manuscript. All authors read and approved the final manuscript.

**Funding** FMdeA, LCH, and SJW were supported by the U.K. Research and Innovation as part of the GCRF, African SWIFT Programme (NE/P021077/1). LCH and SJW were also supported by the National Centre for Atmospheric Science through the NERC National Capability International Programmes Award (NE/X006263/1).

**Data availability** The data used in this research can be found at the following websites: TAMSAT (http://www.tamsat.org.uk/data/); CHIRPS (https://data.chc.ucsb.edu/products/CHIRPS-2.0/global_daily/netcdf/p05/); GPCP (https://rda.ucar.edu/datasets/ds728.7/); TRMM (https://disc2.gesdisc.eosdis.nasa.gov/opendap/TRMM_L3/TRMM_3B42_Daily.7/); S2S hindcasts (https://apps.ecmwf.int/datasets/); RMM index (https://aux.ecmwf.int/ecpds/data/list/RMMS/ (username: s2sidx; passwd: s2sidx)); SubX hindcasts (https://iridl.ldeo.columbia.edu/SOURCES/.Models/.SubX/.NCEP/.CFSv2/.hindcast/.pr/); SST (https://psl.noaa.gov/data/gridded/data.noaa.oisst.v2.highres.html).

**Code availability (software application or custom code)** The python codes used in this research are available upon request to the first author.

## Declarations

**Competing interests** The authors declare no conflicts of interest.

UNCORRECTED PROOF

## References

Ageet S, Fink AH, Maranan M, Diem JE, Hartter J, Ssali AL, Ayabagabo P (2022) Validation of satellite rainfall estimates over equatorial east Africa. J Hydrometeorol 23:129–151. https://doi.org/10.1175/JHM-D-21-0145.1

Allen MP (1997) The t-test for the simple regression coefficient. Understanding Regression Analysis, Springer, 66–70. https://doi.org/10.1007/978-0-585-25657-3_14.

Anande D, Luhunga P (2019) Assessment of Socio-Economic Impacts of the December 2011 Flood Event in Dar es Salaam, Tanzania. Atmospheric Climate Sci 9:421–437. https://doi.org/10.4236/acs.2019.93029

Bahaga TK, Mengistu Tsidu G, Kucharski F, Diro GT (2015) Potential predictability of the sea-surface temperature forced equatorial East African short rains interannual variability in the 20th century. Quart J Roy Meteorol Soc 141:16–26. https://doi.org/10.1002/qj.2338

Bahaga TK, Fink AH, Knippertz P (2019) Revisiting interannual to decadal teleconnections influencing seasonal rainfall in the Greater Horn of Africa during the 20th century. Int J Climatol 39:2765–2785. https://doi.org/10.1002/joc.5986

Behera SK, Luo JJ, Masson S, Delecluse P, Gualdi S, Navarra A, Yamagata T (2005) Paramount impact of the Indian Ocean dipole on the East African short rains: A CGCM study. J Clim 18:4514–4530. https://doi.org/10.1175/JCLI3541.1

Bergonzini L, Richard Y, Petit L, Camberlin P (2004) Zonal circulations over the Indian and Pacific oceans and the level of lakes Victoria and Tanganyika. Int J Climatol 24:1613–1624. https://doi.org/10.1002/joc.1089

Berhane F, Zaitchik B (2014) Modulation of daily precipitation over East Africa by the Madden–Julian oscillation. J Clim 27:6016–6034. https://doi.org/10.1175/JCLI-D-13-00693.1

Black E, Slingo J, Sperber KR (2003) An observational study of the relationship between excessively strong short rains in coastal East Africa and Indian Ocean SST. Mon Weather Rev 131:74–94. https://doi.org/10.1175/1520-0493(2003)131%3c0074:AOSOTR%3e2.0.CO;2

Bowden JH, Semazzi FH (2007) Empirical analysis of intraseasonal climate variability over the Greater Horn of Africa. J Clim 20:5715–5731. https://doi.org/10.1175/2007JCLI1587.1

Camberlin P, Wairoto J (1997) Intraseasonal wind anomalies related to wet and dry spells during the "long" and "short" rainy seasons in Kenya. Theor Appl Climatol 58:57–69. https://doi.org/10.1007/BF00867432

Camberlin P, Moron V, Okoola RE, Philippon N, Gitau W (2009) Components of rainy seasons' variability in equatorial East Africa: Onset, cessation, rainfall frequency and intensity. Theor Appl Climatol 98:237–249. https://doi.org/10.1007/s00704-009-0113-1

Chang'a L, Kijazi A, Mafuru K, Kondowe A, Osima S, Mtongori H, Ng'ongolo H, Juma O, Michael E (2020) Assessment of the Evolution and Socio-Economic Impacts of Extreme Rainfall Events in October 2019 over the East Africa. Atmospheric Climate Sci 10:319–338. https://doi.org/10.4236/acs.2020.103018

de Andrade FM, Young MP, MacLeod D, Hirons LC, Woolnough SJ, Black E (2021) Subseasonal precipitation prediction for Africa: Forecast evaluation and sources of predictability. Weather Forecast 36:265–284. https://doi.org/10.1175/WAF-D-20-0054.1

Dinku T, Ceccato P, Grover-Kopec E, Lemma M, Connor SJ, Ropelewski CF (2007) Validation of satellite rainfall products over East Africa's complex topography. Int J Remote Sens 28:1503–1526. https://doi.org/10.1080/01431160600954688

Dinku T, Ceccato P, Connor SJ (2011) Challenges of satellite rainfall estimation over mountainous and arid parts of east Africa. Int J Remote Sens 32:5965–5979. https://doi.org/10.1080/01431161.2010.499381

FSNAU (Somalia) Food Security & Nutrition Quarterly Brief (2022) — Focus on Post Gu 2017 Season Early Warning (Food Security and Nutrition Analysis Unit and Famine Early Warning System Network)

Funk C, Dettinger MD, Michaelsen JC, Verdin JP, Brown ME, Barlow M, Hoell A (2008) Warming of the Indian Ocean threatens eastern and southern African food security but could be mitigated by agricultural development. Proc Natl Acad Sci 105:11081–11086. https://doi.org/10.1073/pnas.070819610

Funk C, Peterson P, Landsfeld M, Pedreros D, Verdin J, Shukla S, Husak G, Rowland J, Harrison L, Hoell A, Michaelsen J (2015) The climate hazards infrared precipitation with stations—a new environmental record for monitoring extremes. Sci Data 2:150066. https://doi.org/10.1038/sdata.2015.66

Gamoyo M, Reason C, Obura S (2015) Rainfall variability over the East African coast. Theor Appl Climatol 120:311–322. https://doi.org/10.1007/s00704-014-1171-6

Goddard L, Graham NE (1999) Importance of the Indian Ocean for simulating rainfall anomalies over eastern and southern Africa. J Geophys Res Atmos 104:19099–19116. https://doi.org/10.1029/1999JD900326

Gudoshava M, Wanzala M, Thompson E, Mwesigwa J, Endris HS, Segele Z, Hirons L, Kipkogei O, Mumbua C, Njoka W, Baraibar M, de Andrade FM, Woolnough SJ, Atheru Z, Artan G (2022) Application of real-time S2S forecasts over Eastern Africa in the co-production of climate services. Climate Services 27:100319. https://doi.org/10.1016/j.cliser.2022.100319

Hannachi A, Jolliffe IT, Stephenson DB (2007) Empirical orthogonal functions and related techniques in atmospheric science: A review. Int J Climatol: J Royal Meteorol Soc 27:1119–1152. https://doi.org/10.1002/joc.1499

Hendon HH, Wheeler MC, Zhang C (2007) Seasonal dependence of the MJO–ENSO relationship. J Clim 20:531–543. https://doi.org/10.1175/JCLI4003.1

Hersbach H et al (2020) The ERA5 global reanalysis. Q J R Meteorol Soc 146:1999–2049. https://doi.org/10.1002/qj.3803

Hirons L, Turner A (2018) The impact of Indian Ocean mean-state biases in climate models on the representation of the East African short rains. J Clim 31:6611–6631. https://doi.org/10.1175/JCLI-D-17-0804.1

Hirons L, Thompson E, Dione C, Indasi VS, Kilavi M, Nkiaka E, Talib J, Visman E, Adefisan EA, de Andrade FM, Ashong J, Mwesigwa JB, Boult V, Diédhiou T, Konte O, Gudoshava M, Kiptum C, Amoah RK, Lamptey B, Lawal KA, Muita R, Nzekwu R, Nying'uro P, Ochieng W, Olaniyan E, Opoku NK, Endris HS, Segele Z, Igri PM, Mwangi E, Woolnough S (2021) Using co-production to improve the appropriate use of sub-seasonal forecasts in Africa. Climate Services 23:100246. https://doi.org/10.1016/j.cliser.2021.100246

Hoell A, Funk C, Barlow M (2014) La Niña diversity and northwest Indian Ocean rim teleconnections. Clim Dyn 43:1–18. https://doi.org/10.1007/s00382-014-2083-y

Hogan E, Shelly A, Xavier P (2015) The observed and modelled influence of the Madden–Julian Oscillation on East African rainfall. Meteorol Appl 22:459–469. https://doi.org/10.1002/met.1475

Huffman GJ, Adler RF, Morrissey MM, Bolvin DT, Curtis S, Joyce R, McGavock B, Susskind J (2001) Global precipitation at one-degree daily resolution from multisatellite observations. J Hydrometeorol 2:36–50

Huffman GJ, Bolvin DT, Nelkin EJ, Wolff DB, Adler RF, Gu G, Hong Y, Bowman KP, Stocker EF (2007) The TRMM multisatellite precipitation analysis (TMPA): Quasi-global, multiyear, combined-sensor precipitation estimates at fine scales. J Hydrometeorol 8:38–55. https://doi.org/10.1175/JHM560.1

Indeje M, Semazzi FHM, Ogallo LJ (2000) ENSO Signals in East African Rainfall Seasons. Int J Climatol 20:19–46. https://doi.org/10.1002/(SICI)1097-0088(200001)20:1%3c19::AID-JOC449%3e3.0.CO;2-0

Jiang Y, Zhou L, Roundy PE, Hua W, Raghavendra A (2021) Increasing influence of Indian Ocean Dipole on precipitation over Central Equatorial Africa. Geophys Res Lett 48:e2020GL092370. https://doi.org/10.1029/2020GL092370

Kimani MW, Hoedjes JC, Su Z (2017) An assessment of satellite-derived rainfall products relative to ground observations over East Africa. Remote Sensing 9:430. https://doi.org/10.3390/rs9050430

Kolstad EW, MacLeod D (2022) Lagged oceanic effects on the East African short rains. Clim Dyn 59:1043–1056. https://doi.org/10.1007/s00382-022-06176-6

Kolstad EW, Macleod D, Demissie TD (2021) Drivers of subseasonal forecast errors of the East African short rains. Geophysical Res Lett 48:e2021GL093292. https://doi.org/10.1029/2021GL093292

Livezey RE, Chen WY (1983) Statistical field significance and its determination by Monte Carlo techniques. Mon Weather Rev 111:46–59. https://doi.org/10.1175/1520-0493(1983)111%3c0046:SFSAID%3e2.0.CO;2

MacLeod D, Graham R, O'Reilly C, Otieno G, Todd M (2021) Causal pathways linking different flavours of ENSO with the Greater Horn of Africa short rains. Atmos Sci Lett 22(2):e1015. https://doi.org/10.1002/joc.1015

MacLeod D (2019) Seasonal forecast skill over the Greater Horn of Africa: a verification atlas of System 4 and SEAS5—part1/2. ECMWF report. https://www.ecmwf.int/node/18906

Maidment RI, Grimes D, Allan RP, Tarnavsky E, Stringer M, Hewison T, Roebeling R, Black E (2014) The 30-year TAMSAT African rainfall climatology and time series (TARCAT) data set. J Geophysical Res: Atmospheres 119:10–619. https://doi.org/10.1002/2014JD021927

Maidment RI, Grimes D, Black E, Tarnavsky E, Young M, Greatrex H, Allan RP, Stein T, Nkonde E, Senkunda S, Alcántara EM (2017) A new, long-term daily satellite-based rainfall dataset for operational monitoring in Africa. Scientific Data 4:1–9. https://doi.org/10.1038/sdata.2017.63

Mariotti A, Baggett C, Barnes EA, Becker E, Butler A, Collins DC, Dirmeyer PA, Ferranti L, Johnson NC, Jones J, Kirtman BP (2020) Windows of opportunity for skillful forecasts subseasonal to seasonal and beyond. Bull Am Meteor Soc 101:E608–E625. https://doi.org/10.1175/BAMS-D-18-0326.1

Maybee B, Ward N, Hirons LC, Marsham JH (2022) Importance of Madden–Julian oscillation phase to the interannual variability of East African rainfall. Atmospheric Sci Lett 24:e1148. https://doi.org/10.1002/asl.1148

Mutai CC, Ward MN (2000) East African rainfall and the tropical circulation/convection on intraseasonal to interannual timescales. J Clim 13:3915–3939. https://doi.org/10.1175/1520-0442(2000)013%3c3915:EARATT%3e2.0.CO;2

Nicholson SE (2015) Long-term variability of the East African 'short rains' and its links to large-scale factors. Int J Climatol 35:3979–3990. https://doi.org/10.1002/joc.4259

Nicholson SE (2017) Climate and climatic variability of rainfall over eastern Africa. Rev Geophys 55:590–635. https://doi.org/10.1002/2016RG000544

Nicholson SE, Kim J (1997) The relationship of the El Niño-Southern oscillation to African rainfall. Int J Climatol: J Royal Meteorol Soc 17:117–135. https://doi.org/10.1002/(SICI)1097-0088(199702)17:2%3c117::AID-JOC84%3e3.0.CO;2-O

North GR, Bell TL, Cahalan RF, Moeng FJ (1982) Sampling errors in the estimation of empirical orthogonal functions. Mon Weather Rev 110:699–706. https://doi.org/10.1175/1520-0493(1982)110%3c0699:SEITEO%3e2.0.CO;2

Ogallo LJ (1989) The spatial and temporal patterns of the East African seasonal rainfall derived from principal component analysis. Int J Climatol 9:145–167. https://doi.org/10.1002/joc.3370090204

Ogallo LJ, Janowiak JE, Halpert MS (1988) Teleconnection between seasonal rainfall over East Africa and global sea surface temperature anomalies. J Meteorol Soc Jpn 66:807–821. https://doi.org/10.2151/jmsj1965.66.6_807

Omeny PA, Ogallo L, Okoola R, Hendon H, Wheeler M (2008) East African rainfall variability associated with the Madden-Julian Oscillation. J Kenya Meteorol Soc 2:109–118

Palmer PI, Wainwright CM, Dong B et al (2023) Drivers and impacts of Eastern African rainfall variability. Nat Rev Earth Environ 4:254–270. https://doi.org/10.1038/s43017-023-00397-x

Pegion K, Kirtman BP, Becker E, Collins DC, LaJoie E, Burgman R, Bell R, DelSole T, Min D, Zhu Y, Li W et al (2019) The

UNCORRECTED PROOF



| | | | | |
|---|---|---|---|---|
| Journal : **Large 382** | Article No : **7244** | Pages : **17** | MS Code : **7244** | Dispatch : **19-4-2024** |

Subseasonal Experiment (SubX): A multimodel subseasonal prediction experiment. Bull Am Meteor Soc 100:2043–2060. https://doi.org/10.1175/BAMS-D-18-0270.1

Pohl B, Camberlin P (2006a) Influence of the Madden–Julian Oscillation on East African rainfall. I: Intraseasonal variability and regional dependency, Q. J. R. Meteorol. Soc., 132(621), 2521–2539. doi:https://doi.org/10.1256/qj.05.104.

Pohl B, Camberlin P (2006b) Influence of the Madden-Julian Oscillation on East African rainfall: II. March–May season extremes and interannual variability, Q. J. R. Meteorol. Soc. 132(621, B), 2541–2558. https://doi.org/10.1256/qj.05.223.

Reynolds RW, Smith TM, Liu C, Chelton DB, Casey KS, Schlax MG (2007) Daily high-resolution-blended analyses for sea surface temperature. Journal of climate 15;20(22):5473–96. https://doi.org/10.1175/2007JCLI1824.1

Saji NH, Goswami BN, Vinayachandran PN, Yamagata T (1999) A dipole mode in the tropical Indian Ocean. Nature 401:360–363. https://doi.org/10.1038/43854

Schreck CJ, Semazzi FHM (2004) Variability of the recent climate of eastern Africa. Int J Climatol 24:681–701. https://doi.org/10.1002/joc.1019

Sylla MB, Giorgi F, Coppola E, Mariotti L (2013) Uncertainties in daily rainfall over Africa: assessment of gridded observation products and evaluation of a regional climate model simulation. Int J Climatol 33:1805–1817. https://doi.org/10.1002/joc.3551

Trenberth KE, Stepaniak DP (2001) Indices of el Niño evolution. J Clim 14:1697–1701. https://doi.org/10.1175/1520-0442(2001)014%3c1697:LIOENO%3e2.0.CO;2

Ummenhofer CC, Sen Gupta A, England MH, Reason CJ (2009) Contributions of Indian Ocean sea surface temperatures to enhanced East African rainfall. J Clim 22:993–1013. https://doi.org/10.1175/2008JCLI2493.1

Vashisht A, Zaitchik B (2022) Modulation of East African boreal fall rainfall: combined effects of the Madden–Julian oscillation (MJO) and El Niño-Southern Oscillation (ENSO). J Clim 35:2019–2034. https://doi.org/10.1175/JCLI-D-21-0583.1

Vigaud N, Tippett MK, Robertson AW (2018) Probabilistic skill of subseasonal precipitation forecasts for the East Africa-West Asia sector during September–May. Wea Forecasting 33:1513–1532. https://doi.org/10.1175/WAF-D-18-0074.1

Vigaud N, Tippett MK, Robertson AW (2019) Deterministic skill of subseasonal precipitation forecasts for the East Africa–West Asia sector from September to May. J. Geophys. Res. Atmos. 124, 11 887–11 896. https://doi.org/10.1029/2019JD030747

Vitart F (2017) Madden–Julian oscillation prediction and teleconnections in the S2S database. Quart J Roy Meteor Soc 143:2210–2220. https://doi.org/10.1002/qj.3079

Vitart F et al (2017) The Subseasonal to Seasonal (S2S) prediction project database. Bull Amer Meteor Soc 98:163–173. https://doi.org/10.1175/BAMS-D-16-0017.1

Wainwright CM, Finney DL, Kilavi M, Black E, Marsham JH (2021) Extreme rainfall in East Africa, October 2019–January 2020 and context under future climate change. Weather 76:26–31. https://doi.org/10.1002/wea.3824

Walker DP, Birch CE, Marsham JH, Scaife AA, Graham RJ, Segele ZTJCD (2019) Skill of dynamical and GHACOF consensus seasonal forecasts of East African rainfall. Clim Dyn. https://doi.org/10.1007/s00382-019-04835-9

Wenhaji Ndomeni C, Cattani E, Merino A, Levizzani V (2018) An observational study of the variability of East African rainfall with respect to sea surface temperature and soil moisture. Quart J Roy Meteorol Soc 144(S1):384–404. https://doi.org/10.1002/qj.3255

Wheeler MC, Hendon HH (2004) An all-season real-time multivariate MJO index: Development of an index for monitoring and prediction. Mon Wea Rev 132:1917–1932. https://doi.org/10.1175/1520-0493(2004)132%3c1917:AARMMI%3e2.0.CO;2

Wilks D S (2006) Statistical Methods in the Atmospheric Sciences. 2nd ed. International Geophysics Series Vol. 100, Academic Press, 648 pp.

Wilson EA, Gordon AL, Kim D (2013) Observations of the Madden Julian oscillation during Indian Ocean dipole events. Journal of Geophysical Research: Atmospheres 118:2588–2599. https://doi.org/10.1002/jgrd.50241

Zaitchik BF (2017) Madden-Julian Oscillation impacts on tropical African precipitation. Atmos Res 184:88–102. https://doi.org/10.1016/j.atmosres.2016.10.002

Zhang W, Wang Y, Jin F-F, Stuecker MF, Turner AG (2015) Impact of different El Niño types on the El Niño/IOD relationship. Geophys Res Lett 42:8570–8576. https://doi.org/10.1002/2015GL065703

Zhao S, Cook KH (2021) Influence of walker circulations on East African rainfall. Clim Dyn 56:2127–2147. https://doi.org/10.1007/s00382-020-05579-7

**Publisher's Note** Springer Nature remains neutral with regard to jurisdictional claims in published maps and institutional affiliations.

Springer Nature or its licensor (e.g. a society or other partner) holds exclusive rights to this article under a publishing agreement with the author(s) or other rightsholder(s); author self-archiving of the accepted manuscript version of this article is solely governed by the terms of such publishing agreement and applicable law.

UNCORRECTED PROOF

| | |
|---|---|
| Journal: | **382** |
| Article: | **7244** |

# Author Query Form

**Please ensure you fill out your response to the queries raised below and return this form along with your corrections**

Dear Author

During the process of typesetting your article, the following queries have arisen. Please check your typeset proof carefully against the queries listed below and mark the necessary changes either directly on the proof/online grid or in the 'Author's response' area provided below

| Query | Details Required | Author's Response |
|---|---|---|
| AQ1 | Please check if affiliations and there respective authors was captured/presented correctly. | |
| AQ2 | Please confirm if the author names are presented accurately and in the correct sequence (given name, middle name/initial, family name). Author 1 Given name: [specify authors given name] Last name [specify authors last name]. Also, kindly confirm the details in the metadata are correct. | |
| AQ3 | References 'FSNAU 2022, s 2019' are cited in text but not provided in the reference list. Please provide references in the list or delete these citations. | |
| AQ4 | Please check if section heads was captured/presented correctly. | |
| AQ5 | Please check backmatter if all the details in the backmatter was captured/presented correctly. | |
| AQ6 | References 'Chang'a et al (2020), FSNAU (Somalia) Food Security Nutrition Quarterly Brief (2022), Pohl and Camberlin (2006b).' are given in list but not cited in text. Please cite in text or delete them from list. | |
| AQ7 | Please provide complete bibliographic details of references: ( FSNAU (Somalia) Food Security & Nutrition Quarterly Brief (2022) Wilks D S (2006) ) | |